Effect of using regenerative dispalcer on the performance of a beta-type heat engine

E.I. Eid
Mechanical Engg. Dept., Faculty of Industrial Education, Sues Canal University, Suez, Egypt

In this paper, the effect of using the square wire meshes as regenerative media in the displacer space of a beta-type Stirling engine on the engine performance was introduced. Three different configurations of Stirling machines; namely alpha, beta and gamma-configurations, are commonly used. Each configuration has the same thermodynamic cycle but it has different mechanical design arrangements. In the conventional beta-configuration; a displacer and a power piston are incorporated in one cylinder. The displacer transfers the working fluid between expansion and compression spaces via a heater, a regenerator, and a cooler. In the present work, successive homogeneous layers of the square wire meshes will occupy the displacer space in a beta-type engine that make the displacer to be a displacer and a regenerator simultaneously. The theoretical analysis of the proposed engine is mainly based on Schmidt Theory. The main optimum dimensions of the heater, cooler, regenerator, piston stroke, displacer stroke as dimensionless ratios of the bore, the optimum phase angle between the piston and the displacer and the optimum ranges of the speed for each working fluid were found. The present Schmidt model was validated by resolving the technical data of two practical engines and comparing the results from the model with the experimental data of them. The comparison among the proposed engine which has a regenerative displacer and two practical engines having solid displacer and fixed regenerator provided that; the proposed engine gives 16% more power per cc per 1 °C temperature difference between the heat source and the heat sink at a higher speed range than that of the practical SCM81-engine.

في هذا البحث تم دراسة تأثير استخدام مصفوفة السلك المربعة الشكل كمسترجع حرارى فى كاسح محرك حرارى طراز بيتا على أداء المحرك. تتواجد الماكينات التى تعمل وفقا لدورة أسترلنج على شكل ثلاثة تصميمات ميكانيكية مختلفة هم ألفا وبيتا وجاما، كل منهم يعمل وفقا لنفس الدورة. محرك أسترلنج طراز بيتا المتداول يتكون من أسطوانة واحدة تحتوى على مكبس وكاسح ويعمل الكاسح على الكسح الترددى لمائع التشغيل من حيز التمدد الى حيزالانضغاط بالأسطوانة والعكس مارا بمسترجع حراري ثابت. هذا البحث يقترح استخدام طبقات متتالية من مصفوفات السلك المربعة الشكل والمتجانسة لتشغل الحيز الذى يشغله الكاسح المصمت في محرك طراز بيتا وبذلك يؤدى الكاسح وظيفتى الكاسح والمسترجع الحراري فى نفس الوقت بدلا من المسترجع الحراري الثابت في المحرك المتداول. تم عمل التحليل النظري للمحرك المقترح فى ضوء نظرية شميت. هذا وقد أوجدت هذه الدراسة الأبعاد المثلى للمسخن والمبرد والمسترجع الحرارى وطول مشوار المكبس وطول مشوار الكاسح (نسب لابعدية من قطر الأسطوانة) كما أوجدت الدراسة زاوية الطور المثلى والمدى الأمثل لسرعة دوران المحرك عند شحنه بموائع مختلفة (الهواء – النيتروجين – الهيدروجين – الهيليوم). تم التحقق من صلاحية النموذج النظرى (نظرية شميت) وذلك بأخذ المواصفات الفنية لمحركين حراريين عمليين وإعادة حل دورة كل منهما باستخدام النموذج النظرى الحالى. تم حساب القدرة لكل cm^3 لكل $^{\circ}C$ درجة مئوية فرق بين درجتى حرارة كلا من المصدر الحرارى والمصب الحرارى وقد تم مقارنة القدرة المحسوبة والعملية الناتجة من المحركين الحراريين العمليين والمحرك الحرارى المقترح وقد تبين ان المحرك الحرارى الحالى يعطى ١٦% زيادة فى القدرة عن محرك SCM81 العملى وذلك عند مدى أعلى لسرعة الدوران.

Keywords: Stirling engines, Schmidt theory, Beta-type, Wire meshes, Regenerator displacer

1. Introduction

Stirling engine is a simple type of the external-combustion engines that use compressible fluids as working media. Stirling engine is theoretically arranged as a frictionless engine to convert heat into mechanical work at Carnot efficiency. The thermal limit for the operation of a Stirling engine depends on the material used for its construction. In most instances, the engines operate within a heater and cooler temperatures of 923 °K and 338 °K, respectively, [1]. Fig. 1 shows the p–V diagram of an ideal

Stirling cycle with a complete regeneration. The total heat rejected during process 4-1 is absorbed during process 2-3. An external heat sink and heat source are required during processes 1-2 and 3-4 respectively, [2]. The first Stirling machine was built up and tested by Robert Stirling in year 1816 as an alternative to the steam engines and other heat engines. Since Stirling engines are externally heated, they can be powered using a wide variety of fuels and heat sources. On the other hand, the Stirling-cycle refrigerator has no ozone depletion potential, [3]. Referring to fig. 2, three different configurations; namely alpha, beta and gamma-configurations, are commonly used. Each configuration has the same thermodynamic cycle but it has different mechanical design characteristics. In alpha-configuration, twin power pistons; called the hot and cold pistons, are reciprocating in two cylinders. The working fluid fluctuates via heater, regenerator and cooler. In the beta-configuration; a displacer and a power piston are incorporated in the same cylinder. The displacer transfers the working fluid between the hot space and the cold space of the cylinder through the heater, regenerator, and cooler. The gamma-configuration uses two separated cylinders; one for the displacer and the other is for the power piston. The power cylinder connected to the displacer cylinder by using a connection port, [4]. The regenerator design and assembly is difficult to satisfy high effectiveness. Regenerator effectiveness is depended on regenerator surface area, void volume, flow rate, stacking pressure, mesh orientation and screen contamination, [5]. The laminate screen matrix regenerator is fabricated from stainless steel screen sheets that were stacked on top of each other at certain angular orientation. This laminate is porous structure media with highly repeatable properties. On the other hand, the regenerator may be assembled from successive layers of stainless steel wire mesh of different pores/inch and of different wire diameters as indicated by [6]. Homogenous or heterogeneous regenerator can enhance the regenerator effectiveness as well as it may reduce the pressure loss as reported experimentally by [7]. A thermo hydraulic investigation on the packed bed solar air heater having wire screen matrices of different geometrical parameters (wire diameter and pitch) was mathematically modeled by [8]. The thermo hydraulic performance of the air heater was determined from the thermal energy gain subtracted by the energy required to pump air through the packed bed. The results indicated that the packed bed solar air heater is thermo hydraulically efficient as compared to flat plate collectors. The search for an engine cycle with high efficiency, multi-sources of energy and less pollution has led to reconsideration of Stirling cycle. Several engine prototypes were designed but their performances remain relatively weak when compared with other types of combustion engines, [9]. This is due to external and internal conduction, pressure drops in the regenerator and shuttle effect in the pistons. The current researches indicate that Stirling engines that are working with relatively low temperature with helium as working fluid are attractive engines in the future. This is especially related to solar-powered low-temperature differential Stirling engines with double acting, beta and gamma configurations, [10].

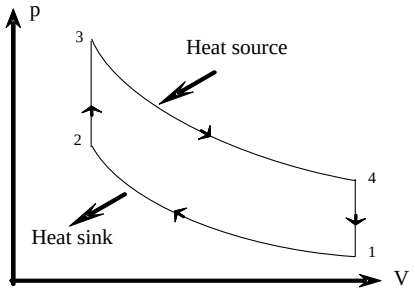

Fig. 1. Ideal Stirling cycle.

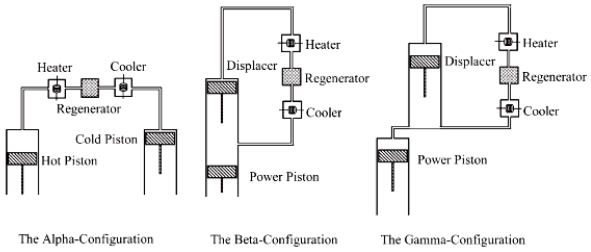

Fig. 2. Different configurations of sterling machines. After [4].

In the present work, the effect of using successive layers of the square wire meshes as

regenerative media that occupy the displacer space in a beta-type Stirling engine on the engine performance will be studied. Referring to fig. 2, the conventional beta-type Stirling engine with a stationary regenerator is clear. However, the proposed beta-type Stirling engine with the regenerative displacer is shown in fig. 3. Where, the working fluid will fluctuate through a reciprocating regenerator instead of the stationary one. The selection of beta-type Stirling engine is referred to its higher specific power rather than alpha and gamma types, [11 and 12]. The selection of wire meshes as regenerative media is due to their rigidity under high pressure, high durability, stability under expansion and compression and their high regeneration effectiveness, [6]. The classical analysis of the operation of the real Stirling engine depends on Schmidt Theory, [13]. This theory is provided for harmonic motion of the reciprocating elements and it retains the assumptions of the isothermal compression and expansion, perfect regeneration and it is certainly more realistic than the ideal Stirling cycle. The present work matches among the more suitable dimensions of the heater, cooler and regenerator, piston stroke, displacer stroke as dimensionless ratios of the cylinder bore for six wire meshes sizes. The effects of the phase angle, charging pressure and speed on the engine performance for each wire mesh size were also exhibited.

2. Beta heat engine

Referring to fig. 3, the proposed beta-configuration heat engine is clear. It consists of a single cylinder with a hot head at the cylinder head, power piston, cooler and a regenerative displacer. It differs from the conventional beta-configuration engine which is shown in fig. 2 in that, the solid displacer piston is replaced by porous regenerative displacer, i.e. the displacer piston performs two jobs; the displacement of the working fluid between expansion and compression spaces and the regenerator job. Thus; the fixed regenerator of the conventional beta-form engine which is shown in fig. 2 is replaced by a reciprocating regenerator (regenerative displacer) as shown in fig. 3. This was identified as an idea for gamma type Stirling engine by [11]. The synchronization of the reciprocation of both power piston and displacer is controlled by using a rhombic drive mechanism. Fig. 4 shows a schematic diagram of the rhombic drive mechanism with power piston and displacer are connected to the cross bars *c'b'* and *cb*, respectively. Two inter-meshing gears are used to keep the synchronization of the reciprocation of both, [14]. The dimensions of the links of the mechanism are as shown in fig. 4. The position, velocity and acceleration vector of each link of the drive mechanism can be determined as follows:

$$\bar{r}_{ao} = (r_g - r)\cos\phi\,\bar{i} + r\sin\phi\bar{j}\,, \tag{1}$$

$$\bar{v}_{ao} = \frac{d\bar{r}_{ao}}{dt} = -(r_g - r)w\sin\phi_1 + rw\cos\phi\bar{j}, \tag{2}$$

$$\bar{r}_{bo} = \bar{r}_{ba} + \bar{r}_{ao} = [r_1\cos\phi_i + (r_g - r)\cos\phi]\bar{i}, \tag{3}$$

$$\bar{v}_{bo} = \frac{d\bar{r}_{bo}}{dt} = [-r_1w_1\sin\phi_1 - (r_g - r)w\sin\phi]\bar{i} + (\bar{r}_1w_1\cos\phi_i + rw\cos\phi)\bar{j}\,, \tag{4}$$

$$\bar{r}_{bo} = \bar{r}_{ba} + \bar{r}_{ao} = [r_1\cos\phi_i + (r_g - r)\cos\phi]\bar{i} \quad \bar{i}_1 + (r_2\sin\phi_2 + r\sin\phi)\bar{j}\,. \tag{5}$$

Similarly;

$$\bar{v}_{b'o} = \frac{d\bar{r}_{b'o}}{dt} = (-r_2w_2\sin\phi_2 - (r_g - r)\, w sin\phi]\ \bar{i} + (r_2w_2\cos\varphi_2 + r\sin\varphi]\bar{j} \quad . \tag{6}$$

As x-component of $\bar{r}_{bo}$ is constant, i.e. $[r_1\cos\phi_1 + (r_g - r)\cos\phi] = r_3/2$ hence;

$$\phi_1 = \cos^{-1}[\{r_3/2 - (r_g - r)\cos\phi\}/r_1. \tag{7}$$

And as a consequence, the y-component of $\bar{r}_{bo}$ which is the displacer movement y_b, is:

$$Y_b = r_1\ sin\ \phi + r\ sin\ \phi\ . \tag{8}$$

Similarly;

$$\phi_2 = \cos^{-1}[\{r_3/2 - (r_g - r)\cos\phi\}/r_2]. \quad (9)$$

The y-component of $\bar{r}b'o$ which is the piston movement $\bar{r}b'o$, which is the piston movement yb' is:

$$yb' = r_2 \sin\phi_2 + r\sin\phi \quad . \quad (10)$$

Fig. 5 shows the cyclic movement of both piston and displacer, from which one can get piston and displacer strokes as well as the phase angle shift between them. Also, the swept volume of both expansion and compression spaces can be stated. Thus; the variation of both expansion and compression spaces are as follows:

$$V_E = (V_{SE}/2)\, x\,(1 + \cos\phi) + V_{cl..E.} \quad (11)$$

$$V_C = (V_{SE}/2)\, x\,(1 + \cos\phi) + (V_{SC}/2)\, x\,(1 - \cos(\phi - \alpha)\} + V_{cl,C} + V_{PO}. \quad (12)$$

The engine work space is divided into three isothermal regions in the vision of Schmidt Theory, [13]. The expansion and heater spaces are at the higher temperature T_E, the compression and positive overlap spaces are at the lower temperature T_C and the regenerator space at an intermediate temperature T_R which is expressed as follows:

$$T_R = (T_E - T_C) / \ln(T_E / T_C). \quad (13)$$

According to Schmidt Theory; the instantaneous pressure is kept constant throughout the engine work space, and as a consequence, the mass of the charged working fluid is:

$$m_t = (m_E + m_h) + m_R + (m_C + m_{PO})$$

$$= \frac{p(V_E + V_h)}{RT_E} + \frac{p(V_R)}{RT_R} + \frac{p(V_C + V_{pO})}{RT_C}. \quad (14)$$

Thus; the Schmidt pressure is:

$$p = \frac{m_t R T_E}{\left[(V_E + V_h) + \frac{\ln(1/\xi)}{1-\xi}(V_R) + \frac{1}{\xi}(V_C + V_{po})\right]}. \quad (15)$$

The cyclic Schmidt p-V is represented in fig. 6. Referring to fig. 3; and applying the mass conservation equation between the different spaces of the engine workspace, [15];

For the heater space;

$$\frac{dm_h}{dt} = 0 - m_{h\to E} \quad . \quad (16)$$

For the expansion space;

$$\frac{dm_h}{dt} = 0 - m_{h\to E} - \dot{m}_{E\to R} \quad (17)$$

For the regenerator space;

$$\frac{dm_R}{dt} = \dot{m}_{E\to R} - \dot{m}_{R\to PO} \quad (18)$$

For the positive overlap and compression spaces:

$$\frac{dm_C}{dt} = \dot{m}_{R\to PO} - 0 \quad (19)$$

From the eqs. (16-19); one can find; $\dot{m}_{h\to E}, \dot{m}_{E\to R}$ and $\dot{m}_{R\to PO}$. Hence the flow rate through the heater, the regenerator and the cooler can be found as follows;

$$\dot{m}_h = \dot{m}_{E\to h} \quad (20)$$

$$\dot{m}_R = (\dot{m}_{E\to R} + \dot{m}_{R\to PO})/2 \quad . \quad (21)$$

$$\dot{m}_k = \dot{m}_{R\to PO}. \quad (22)$$

Fig. 7 shows the cyclic mass fluctuations via the heater, the cooler and the regenerator during a complete cycle of the engine. Thus, the instantaneous Reynolds numbers through the heater, the regenerator and the cooler are as follows:

1- Flue gases
2- Hot head
3- Expansion space
4- Regenerative displacer
5- Engine cylinder
6- Displacer rod
7- Cooling water jacket
8- Power piston
9- Cooling water inlet
10- Cooling water outlet
11- Piston rod
12- Displacer cross bar
13- Connecting rod (four-ones)
14- Intermeshing gear (two-ones)
15- Crank shaft (two-ones)
16- Piston cross bar

E	Expansion space
R	Regenerative displacer
PO	Positive over-lap space
C	Compression space
TDC	Top dead center
BDC	Bottom dead center
L_{cl}	Clearance gap
S_d	Displacer stroke
S_p	Piston stroke
L_{PO}	Positive over-lap space height
D	Cylinder bore
H_h	Hot head height
H_R	Regenerator height

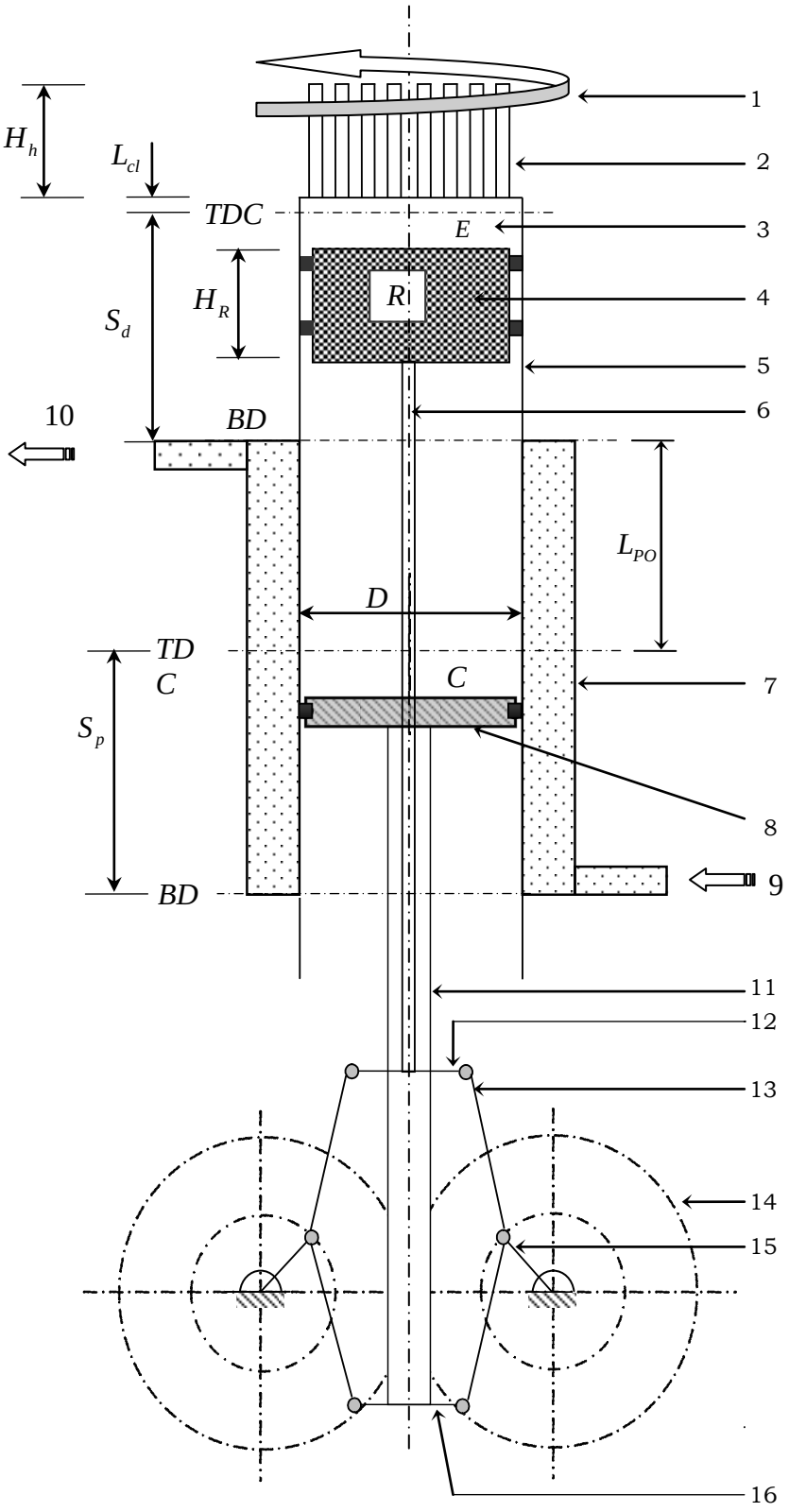

Fig. 3. Scheme of the proposed beta-type stirling engine.

O	Origin
o`	Crank shaft axis
a	Crank shaft pin
ab	Displacer connecting rod
bc	Displacer cross bar
ab`	Piston connecting rod
b`c`	Piston cross bar
r	Crank shaft radius
r_1	Displacer connecting rod length
r_2	Piston connecting rod Length
r_3	Cross bar length
r_g	Intermeshing gear radius
ϕ	Crank angle
ϕ_1	Displacer connecting rod angle
ϕ_1	Piston connecting rod angle
y_b	Displacer movement
$y_{b'}$	Piston movement

$$x_b = x_{b`} = \frac{r_3}{2}$$

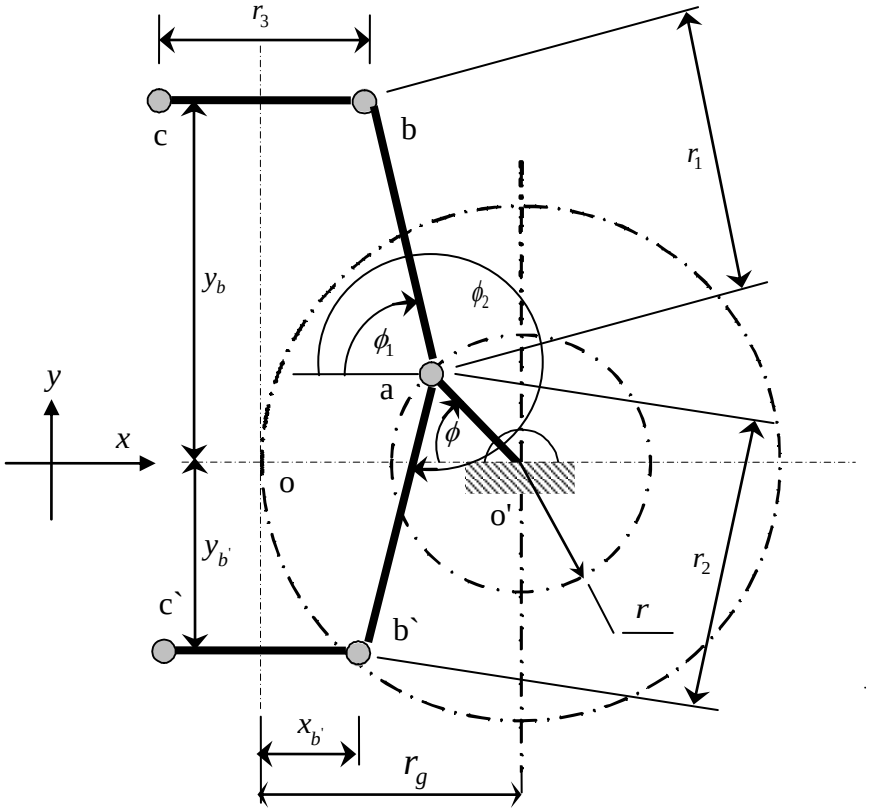

Fig. 4. Dimensions and angles of rhombic drive.

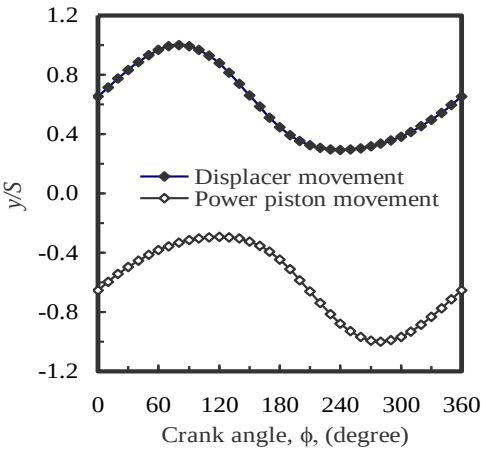

Fig. 5. Piston and displacer movement versus crank angle.

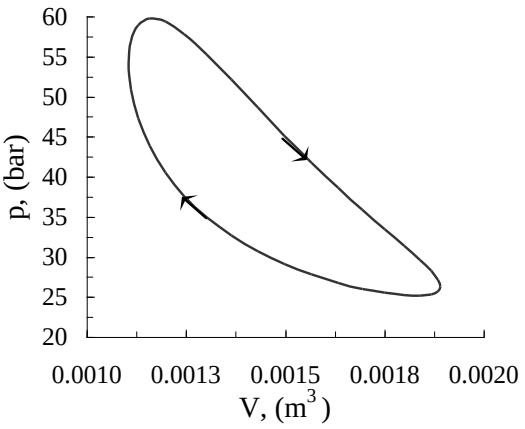

Fig. 6. Schmidt p-V diagram at a charging pressure of 20 bar.

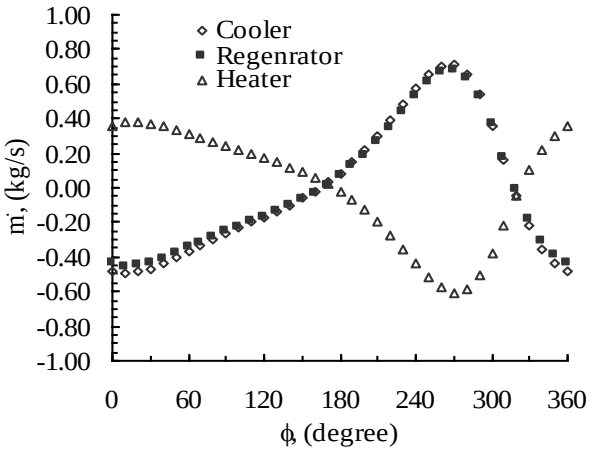

Fig. 7. Cyclic mass flow rate variation through cooler, heater and regenerator.

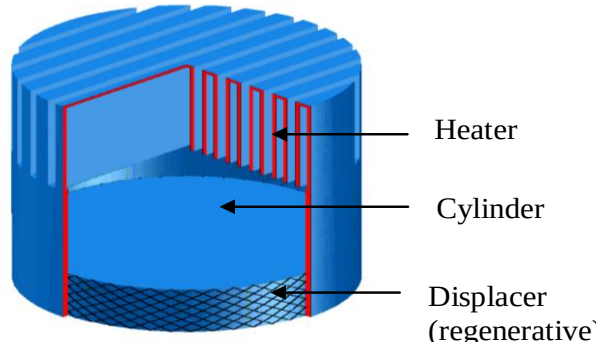

Fig. 8. Half-cross-section in the heater and cylinder.

$$\mathrm{Re}_h \; \dot{m}_h \times H_h / (\mu_E / a_h) \; . \tag{23}$$

$$\mathrm{Re}_R \; \dot{m}_R \times d_{hyd,R} / (\mu_R / a_R) . \tag{24}$$

$$\mathrm{Re}_K \; \dot{m}_k \times d_k / (\mu_C / a_k) . \tag{25}$$

2.1. Heater

The suggested heater for the proposed engine is as the one which was experimentally tested by [16]. The suggested heater is inverted U-shaped stainless steel cups that can be heated externally by the exhaust gases as shown in fig. 8. The data from experimental tests of such heaters were concluded that the overall heat transfer coefficient during a complete cycle is; U = 311 W/m^2 °C for the exhaust of LPG fuel at a temperature of T_f = 600 °C, for air as a working fluid. Thus;

$$Q_h = U \, A_{h,o} \; (T_f - T_E) \; . \tag{26}$$

The pressure drop through the heater is, [17]:

$$\Delta ph = 1.6 \times [K \times \rho \times v^2 / 2]_h . \tag{27}$$

2.2. Regenerator

The regenerative displacer has a cylindrical shape, as shown in fig. 8. The regenerator is formed from successive layers of stainless steel wire meshes having the same mesh size. The meshes layers were homogenously stacked on the top of each other without revolving angle between any two successive layers and without a stacking pressure upon all. Referring to fig. 9, six meshes of different pitch and different wire diameters were suggested to be used in the proposed regenerative displacer; their technical data are given in table 1, [6].

The pressure drop through the regenerative displacer is, [18]:

$$\Delta pR = [f \times (H / d_{hd}) \times \rho \times v^2 / 2]_R \tag{28}$$

Where;

$$d_{hyd} = [(1 - \psi] \times d_w \tag{29}$$

The friction factor, f, is given as follows, [18]:

$$\log (f_R) = 1.73 - 0.93 \log (\mathrm{Re}_R) \tag{30}$$

If $0 < Re_R \leq 60$

$$\log (f_R) = 0.714 - 0.365 \log (\mathrm{Re}_R) \tag{31}$$

Table 1
Technical data of meshes

Mesh-i	d_w, (mm)	Porosity; ψ (%)
Mesh-50	0.200	69.08
Mesh-100	0.112	65.37
Mesh-200	0.050	69.08
Mesh-300	0.030	72.17
Mesh-400	0.030	62.89
Mesh-500	0.025	61.35

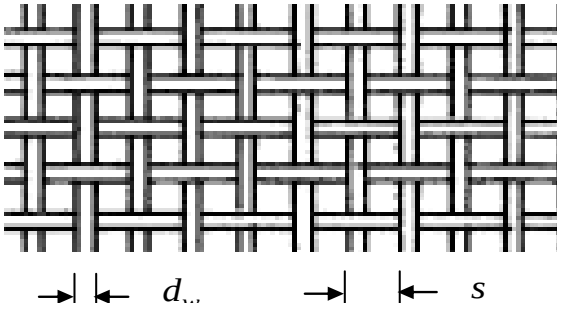

Fig. 9. Schematic diagram of the wire mesh. (After, [6]).

If $60 < Re_R \le 1000$

$\log (f_R) = 0.015 - 0.125 \log (Re_R)$

If $Re_R \le 1000$. (32)

The regenerator effectiveness is, [18]:

$$\varepsilon = NTU_R / (1 + NTU_R). \quad (33)$$

$$NTU_R = 2 \times \bar{St}_R \times H_R / d_{hyd,R} \quad (34)$$

And

$$St_R = 0.595 / Re_R^{0.4} \times Pr_R \quad (35)$$

2.3. Cooler

A water-jacket about the compression space in the engine cylinder was selected to be a cooler in the proposed engine. The working fluid is cooled during its fluctuation through the compression space. The cooling rate is, [19]:

$$\begin{aligned} \dot{Q}_k &= h_o A_{k,o} (T_{k,o} - T_w) \\ &= 2\ \pi k_k L_k (T_{k,i} - T_{k,o}) / \ln(d_{k,o} / d_{k,i}) \\ &= h_i A_{k,i} (T_C - T_{k,i}). \end{aligned} \quad (36)$$

The pressure drop through the cooler tubes is as follows, [17]:

$$\Delta p_k = 1.6[fL/d) \times \rho \times v^2 / 2]_k \quad (37)$$

3. Power and efficiency

The elliptic p-V diagram for both expansion and compression spaces when taken the pressure losses into consideration is illustrated in fig. 10. The indicated power is as follows, [12]:

$$Pind = N \times \left[\oint p_E dV_E + \oint p_C dV_C \right]. \quad (38)$$

The rate of heat added is:

$$Q_h = N \times \oint p_E \, dV_E . \quad (39)$$

The indicated efficiency is:

$$\eta_{ind} = P_{ind} / \dot{Q}_h . \quad (40)$$

A computer program in the form of a spreadsheet was prepared on the Microsoft EXCEL to compute the instantaneous volumes of expansion and compression spaces, instantaneous mass flow rates through the three heat exchangers, instantaneous Reynolds numbers in the heat exchangers, heat transfer rates, pressure drop, indicated power and efficiency. This was done for a complete revolution of the crank at a step of 1 *degree* of the crank angle ϕ. Throughout the calculations, it was assumed that the engine works between two constant higher and lower temperature limits of T_{max} = 600 °C and T_{min} = 80 °C and the cylinder bore is constant at 100 *mm*.

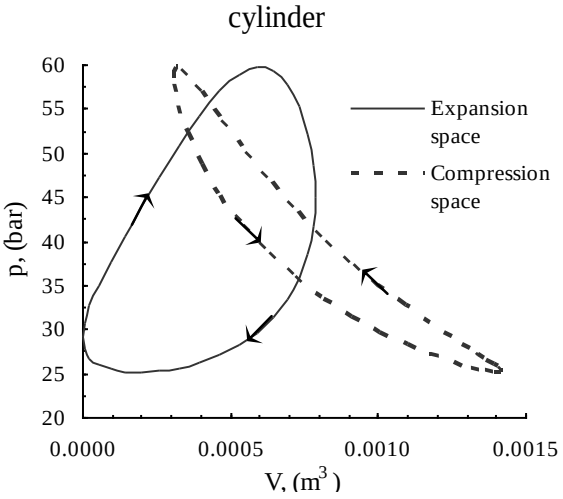

Fig. 10. p-V diagram for both expansion and compression

The program has the possibility to vary the dimensions of the heater, cooler, regenerator, piston stroke and displacer stroke as dimensionless ratios of the cylinder bore for each mesh size. Also, it can optimize the phase angle, charging pressure and speed for each mesh size and for the type of the working fluid.

4. Results and discussion

The results of the present work aim at the clarification of the influence of the dimensions of the inverted U-cub heater, regenerator and cooler as dimensionless ratios of the bore on the performance of the proposed engine. Also, the effects of stroke to bore ratio for both piston and displacer, phase angle, charging pressure, speed and working fluid on the performance of the proposed engine were also exhibited.

The heater height to bore ratio, H_h/D was changed from 0.75 to 1.55 at a step of 0.1 each, and the corresponding values of both indicated power and efficiency were determined. Fig. 11 shows a higher rate of increase in the power with the increase of the heater height ratio up to about 1.0. Beyond this value, the rate of increase of the power is reduced some how. This is referred to the increase in the heat transfer area; however, further increase in the heater height causes an increase in the dead volume space which reduces both compression and pressure ratios that decrease the power. Also, thin wire meshes cause higher pressure losses than the thick ones that reduce the power as shown in fig. 11. The same tendency is even remarked in fig. 12 for the indicated efficiency versus the height of the heater. Therefore; the heater height was chosen at H_h/D = 1 for each wire mesh size.

For the same displacer height, the thin wire meshes show more decrease in the power than that of thick ones as shown in fig. 13. This due to, the thin wire meshes have more pores/inch that reduce both pitch and free flow area, and as a consequence, the flow velocity and pressure losses increase. The increase in the pressure losses reduces the area of the p-V cycle which reduces the work/cycle and power. The increase in the displacer height increases the engine work space and the charged mass of the working fluid will increase which raises the indicated power. Also, the increase in the displacer height increases the regenerator effectiveness which raises the power. The indicated efficiency is slightly increased as the displacer height increases as shown in fig. 14.

Increasing piston stroke to bore ratio increases the mass of the charged fluid, which increases the indicated power up to about S_p/D, as shown in fig. 15. Beyond this value, the more increase in the piston stroke increases the total charged mass of the fluid

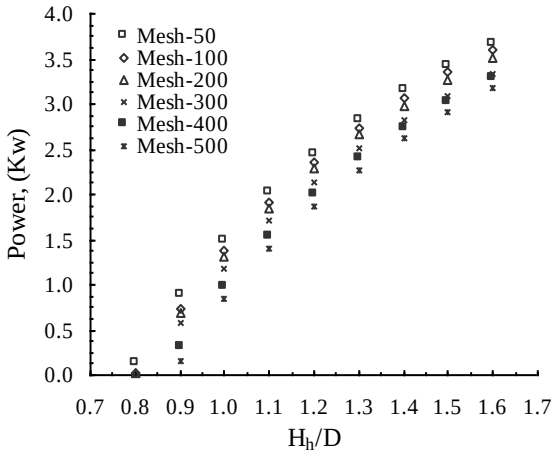

Fig. 11. Variation of power versus heater height for different wire-meshes.

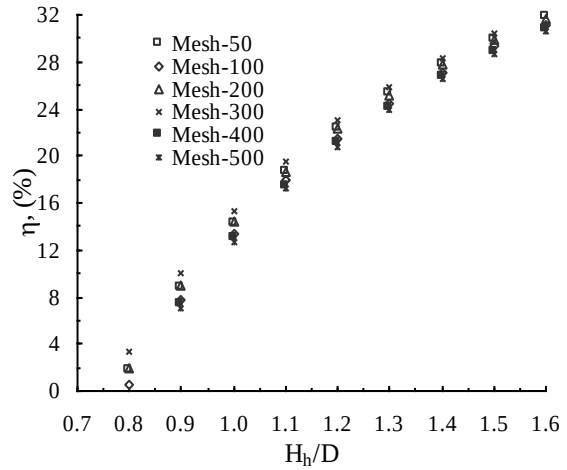

Fig. 12. Variation of power versus heater height for different wire-meshes.

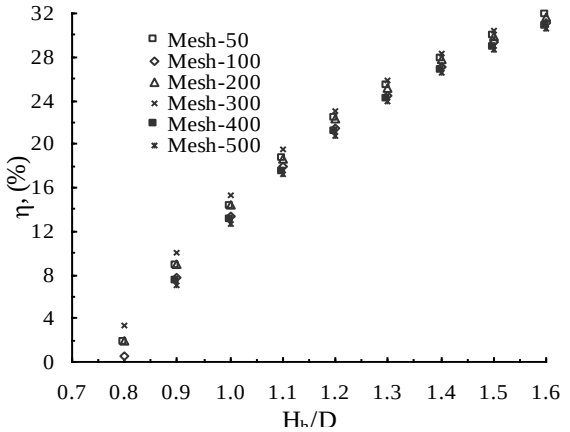

Fig. 13. Variation of power versus displace height for different wire-meshes.

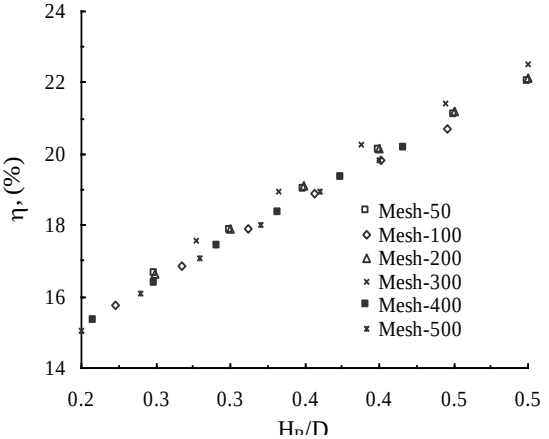

Fig. 14. Variation of efficiency versus displacer height for different wire-meshes.

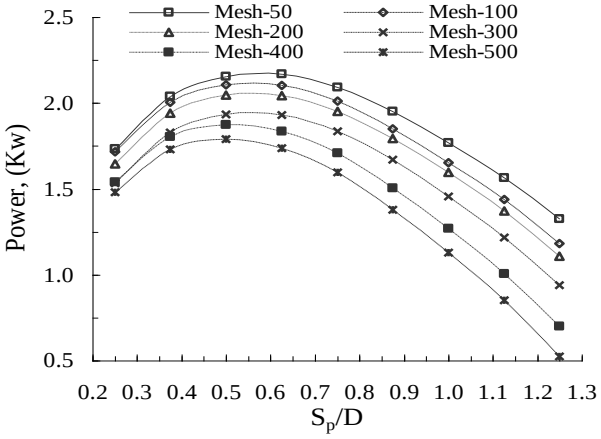

Fig. 15. Variation of power versus piston stroke for different wire-meshes.

which results in high flow velocity and high pressure drop throughout the heater, regenerator and cooler and as a consequence the power decreases. The efficiency decreases as the piston stroke increases as shown in fig. 16. This due to the increase in the heat rejected by the cooler resulted from the increase in its surface area. Referring to fig. 17, it is obvious that each wire mesh size has an optimal value of the displacer stroke to bore ratio as the following:

Mesh size	50	100	200	300	400	500
S_d / D	5	4	3	2	2	2

Increasing displacer stroke increases the total charged mass inside the engine workspace which will increase the power delivered. Further increase in the displacer stroke causes an increase in the pressure losses through the regenerator and this drop is highly increased as increasing the mesh size number. This is why the optimum displacer stroke to bore ratio decreases as the mesh size increases. The increase in the cycle work resulted from the increase of displacer stroke is clear in fig. 18. Where as the increase in the displacer stroke resulted in an increase in the elliptic p-V area for a mesh size of 100 pores/inch.

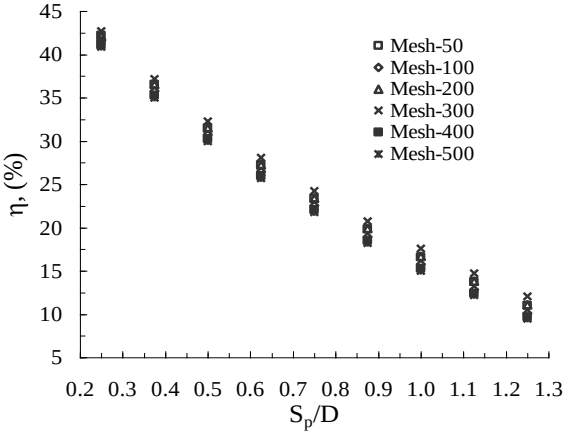

Fig. 16. Variation of efficiency versus piston stroke for different wire-meshes.

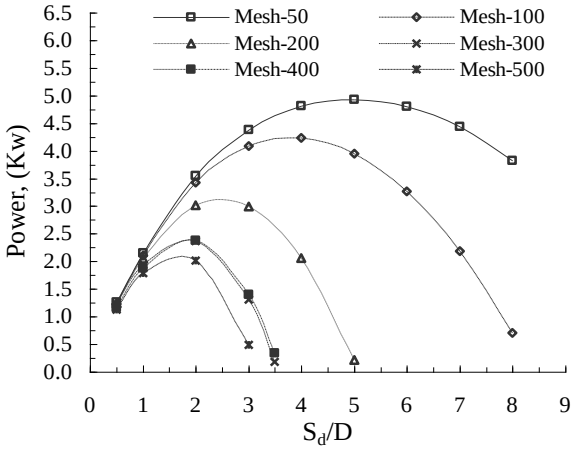

Fig. 17. Variation of power versus displacer stroke for different wire-meshes.

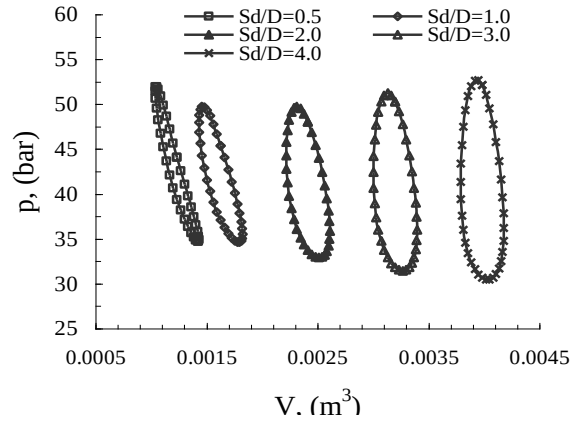

Fig. 18. Schmidt p-V diagram for different displacer strokes for mesh 100.

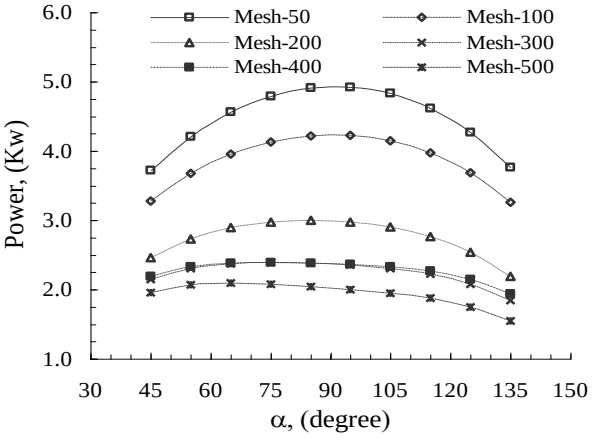

Fig. 19. Variation of power versus phase angle for different wire-meshes.

The change of the phase angle between the piston and the displacer can be done by the changing of the dimensions of the rhombic drive mechanism, [20]. The change in the phase angle resulted in a change of both compression and pressure ratios that affect the work per cycle and consequently the power. The phase angle was varied from 45 degree to 135 degree for the six wire meshes. Referring to fig. 19, it is evident that the more optimum phase angle for most of wire mesh sizes is about 90 degree, which is corresponding to maximum pressure and compression ratios. Also, the increase in the compression and pressure ratios increase the temperature in both compression and expansion spaces that increase the heat rejection rate and reduce the heat addition rate and as a consequence the efficiency will decrease as shown in fig. 20.

Figs. 21, 23, 25 and 27 provide the variation of the power with the engine speed when the engine is charged with air, nitrogen, hydrogen and helium respectively for the six wire meshes. These results were obtained at a charging pressure of 20 *bar* and using the optimum dimensions of heater, cooler, regenerator, piston stroke, displacer stroke and phase angle for each wire mesh size. The range of the optimum engine speed for each working fluid and wire mesh size leads to an acceptable efficiency as shown in figs. 22, 24, 26 and 28.

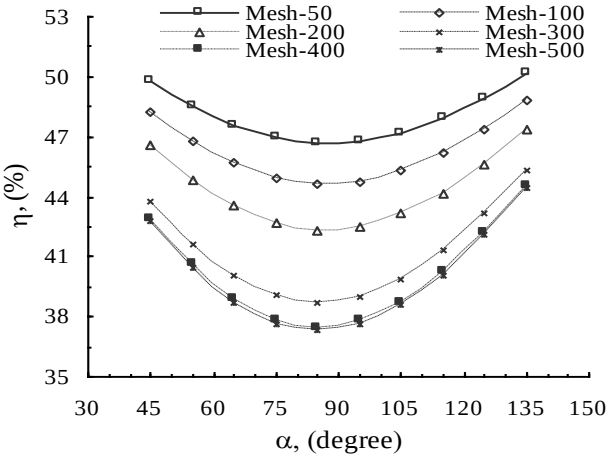

Fig. 20. Variation of efficiency versus phase angle for different wire-meshes.

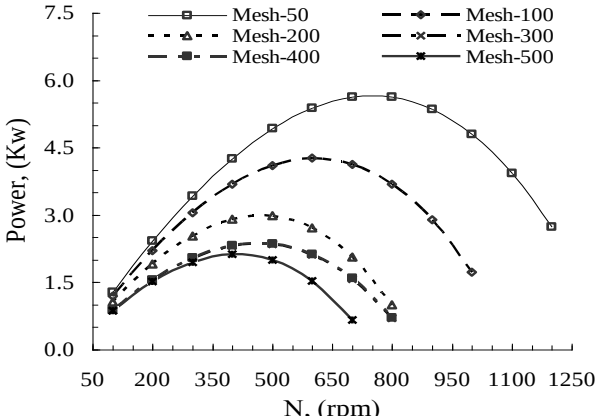

Fig. 21. Variation of power versus the speed for air a working fluid.

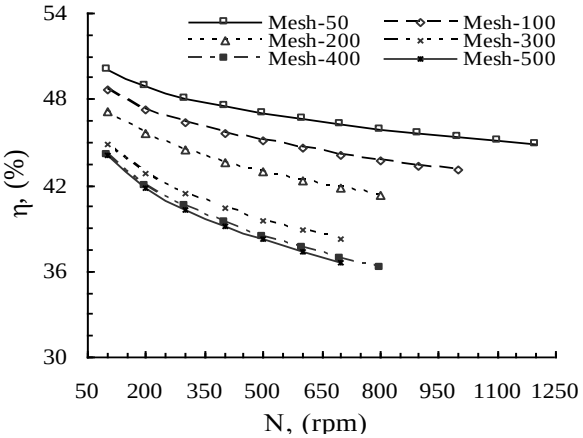

Fig. 24. Variation of efficiency versus the speed for nitrogen as a working fluid.

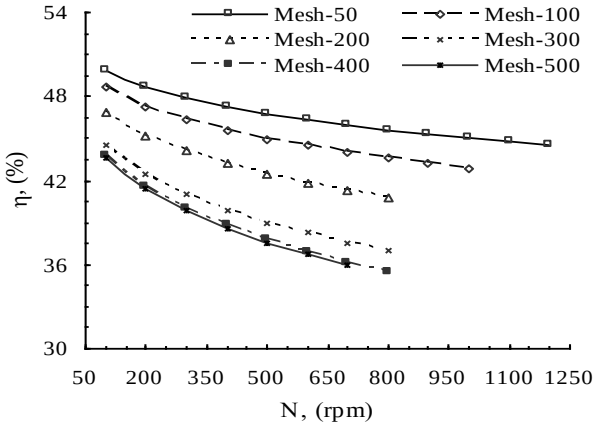

Fig. 22. Variation of efficiency versus the speed for air as a working fluid.

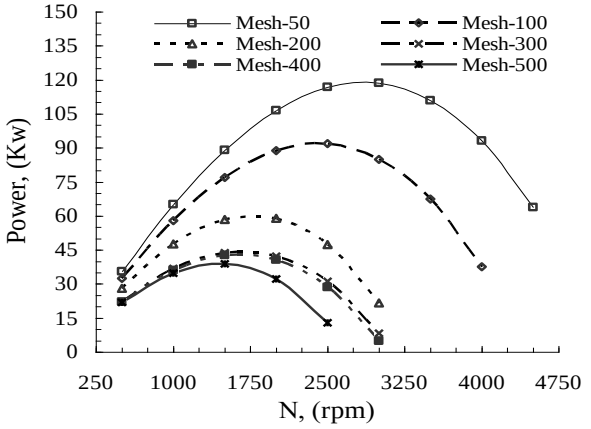

Fig. 25. Variation of power versus the speed for hydrogen as a fluid.

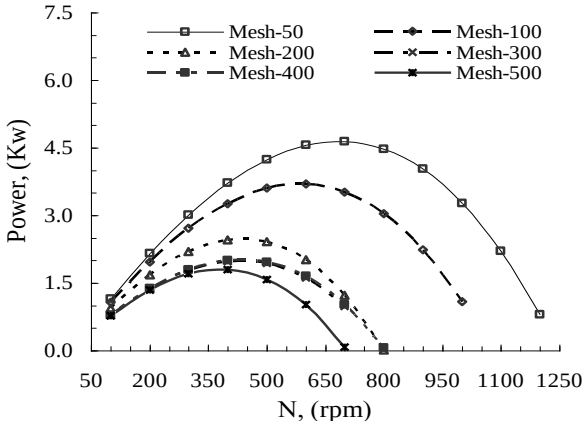

Fig. 23. Variation of power versus the speed for nitrogen as a working fluid.

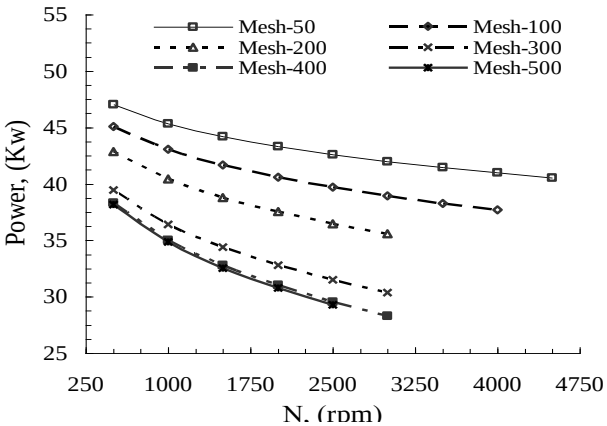

Fig. 26. Variation of efficiency versus the speed for hydrogen as a working fluid.

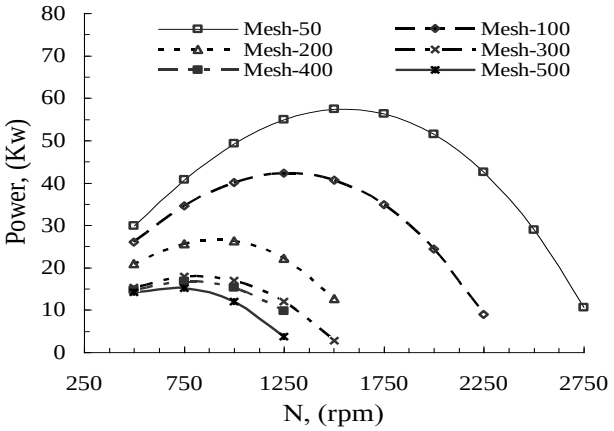

Fig. 27. Variation of power versus the speed for helium as a working fluid.

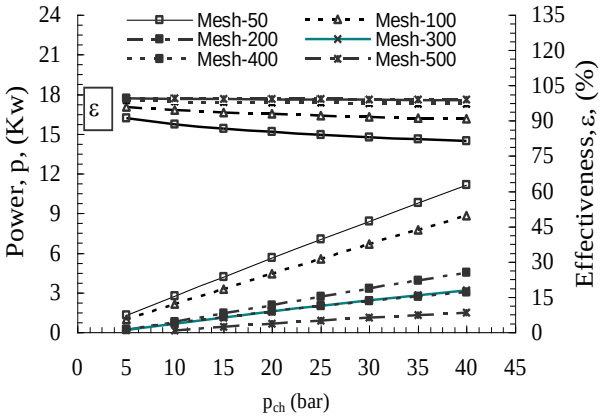

Fig. 29. Variation of power versus charging pressure with air is the working fluid.

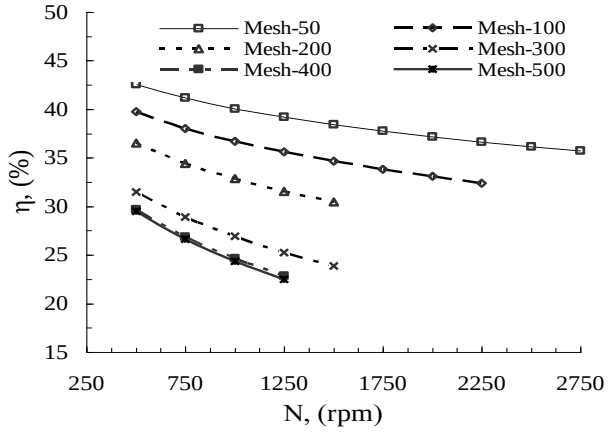

Fig. 28. Variation of efficiency versus charging pressure with air is the working fluid.

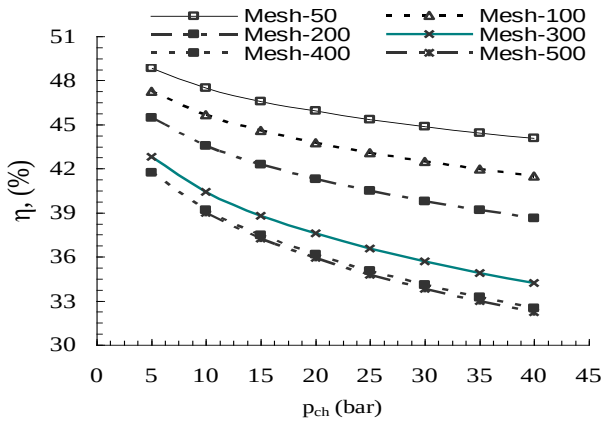

Fig. 30. Variation of efficiency versus charging pressure with air is the working fluid.

Regardless of the working fluid leakage and the shortage in the life time of the piston rings, one can say; the more increase in the charging pressure, the more increase in the power delivered as shown in fig. 29. This is due to, the increase in the total charged mass of the working fluid within the engine workspace. However, the increase in the charging pressure resulted in a decrease in the indicated efficiency as shown in fig. 30. This is due to the reduction in the regenerator effectiveness which is represented in fig. 29; which increases the compression space temperature and decreases the expansion space temperature, and as a consequence the efficiency decreases.

5. Comparison among present work and previous ones

The urgent need to renewable energies has led to the development of Stirling engines, that have an excellent theoretical efficiency, equivalent to Carnot. They can use any source of energy and they are less polluting than the traditional engines. The experimental performance of SCM81 Stirling engine had been done by [21].The SCM81 engine was heated by a heat source of $750\,^{0}C$ and it was cooled by a heat sink of $40\,^{0}C$. The engine has 72 mm bore, 20 mm stroke and it uses Helium as a working fluid. Also, a heat recovery Stirling engine which uses the exhaust gases from a Diesel engine of a freight

ship was tested experimentally by [22]. This engine has 100 *mm* bore, 32 *mm* displacer stroke and 28 *mm* piston stroke. It uses Helium as a working fluid. The heat source (exhaust gases) is at 400 °C and the coolant water is at 40 °C. Both practical engines of [21 and 22] are having a fixed regenerator and solid displacer. For the checking of the validation of the present model, the technical data of the engines of [21 and 22] were resolved to get the developed power and efficiency by using the present Schmidt model. The powers developed from the proposed engine and engines of [21 and 22] were calculated per cc per 1°C temperature differential between the heat source and the heat sink, ΔT. Referring to figs. 31 and 32, and comparing the results from the model with the experimental results of engines of [21 and 22], it is noted a quite fare validation for the present Schmidt model. Moreover, it is also obvious that the proposed engine which having a regenerative displacer delivers higher power at higher speed range than the engines having solid displacer and fixed regenerator.

6. Conclusions

In the present work, the effect of using successive homogeneous stainless steel wire meshes to be filled the space of the displacer of a beta-type Stirling engine, instead of solid one, on its performance was exhibited. The porous displacer will perform as a displacer and as a regenerator simultaneously instead of both solid displacer and stationary porous regenerator. Six wire meshes of different mesh size were suggested to be the regenerative media. The analysis of the engine performance is mainly based on Schmidt Theory. The optimum dimensions of heater, cooler, regenerator, piston stroke, displacer stroke as dimensionless ratios of the cylinder bore, the optimum phase angle between the piston and the displacer and the optimum ranges of the speed for each working fluid were stated. The main concluded remarks of the present work can be systemized as follows:

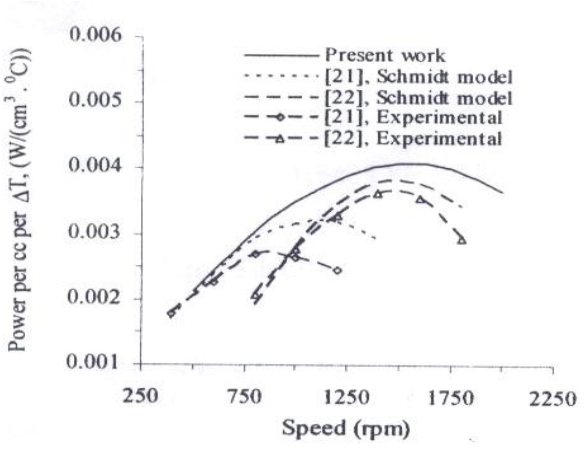

Fig. 31. Comparison of the power per cc per °C versus speed among present work and previous works.

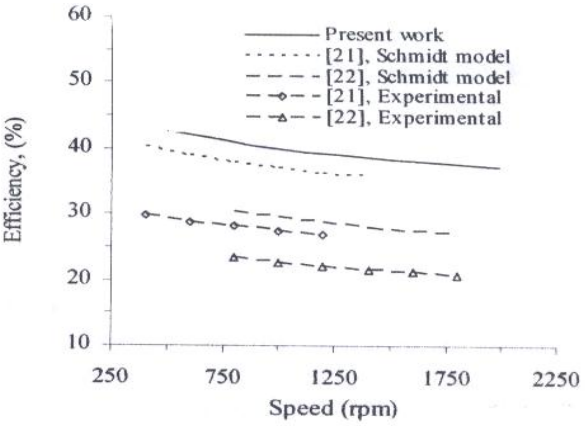

Fig. 32. Comparison of the efficiency versus speed among present work and previous works.

1. The proposed beta-engine which has a regenerative porous displacer instead of both solid displacer and a stationary regenerator delivers 16% more power per cc per 1°C of ΔT, than that from the tested SCM81 Stirling engine which has a stationary regenerator and solid displacer with an increase in the efficiency by about 15%.
2. The present analysis suggested successive layers of homogenous wire meshes of different mesh sizes. However, the present model allows the using of successive layers of heterogeneous wire meshes as well as the using of other types of regenerative media.
3. The replacement of the stationary regenerator by a reciprocating regenerative

displacer incorporated inside the engine cylinder will reduce the total space occupied by the engine as well as it will slightly reduce the engine weight.

The present work exhibits approximate design dimensions of a beta-type engine as dimensionless ratios of the bore. And as a consequence, the engine size can be adapted to be standard selected codes.

Nomenclature

A	Surface area, m^2
a	Cross-section area, m^2
cc	Cubic centimeter,
D	Cylinder bore, m
d	Diameter,
f	Frication,
H	Height,
S	Stroke m
h	Heat transfer coef, $W/m^2.K$
$\underline{i}$	Wire mesh, pores/inch
$\vec{i}, \vec{j}$	Cartesian unit vectors
K	Minor losses factor
k	Thermal conductivity W/m.K
L	Length, m
m	Mass, kg
m	Mass flow rate, kg/s
N	Speed, rps
NTU	Number of transfer units
P	Power, W
P	Pressure, N/m^2
Q	Heat transfer rate, W
R	Specific gas constant, J/kg.K
Re	Reynolds number,
$\bar{r}$	Position vector, m
T	Temperature, K
t	Time, s
U	Overall heat transfer coefficient, $W/m^2.K$
V	Volume, m^3
v	Velocity, m/s
$\vec{v}$	Velocity vector, m/s
	Angular velocity,
x, y	Cartesian coordinates,
α	Phase angle, rad
ΔT	Temperature difference between heat source and heat sink, K
ε	Regenerator effectiveness
ϕ	Crank angle rad.
η	Efficiency
μ	Dynamic viscosity, $pa.s$
ξ	Temp, ratio = T_C/T_E
ρ	Density, kg/m^3
ψ	Porosity
C	Compression space,
cl	Clearance
ch	Charging
d	displacer
E	Expansion space
f	Flue gases
g	Intermeshing gear
h	Heater
hyd	Hydraulic
I	Inner conditions
Ind	Indicated
k	Cooler
o	Outer conditions
p	Piston
PO	Positive overlap
R	Regenerator
SE	Swept expansion
SC	Swept compression
t	Total
w	Wire

References

[1] G. Walker Stirling Engines, Oxford: Clarendon Press (1980).

[2] B. Kongtragool and S. Wongwises, Technical note: Thermodynamic Analysis of a Stirling Engine Including Dead volumes of Hot Space, Cold Space and Regenerator, Renewable Energy, Vol. 31, pp. 345–359 (2006).

[3] O.A. Ataer and H. Karabulut, Thermodynamic Analysis of the V-type Stirling-Cycle Refrigerator, Int. J. of Refrigeration, Vol. 28, pp. 183–189, (2005).

[4] B. Kongtragool and S. Wongwises, A Review of Solar-Powered Stirling Engines and Low Temperature Differential Stirling Engines, Renewable and Sustainable Energy Reviews, Vol. 7, pp. 131–154 (2003).

[5] U. Bin-Nun and D. Manitakos, Low Cost and High Performance Screen Laminate Regenerator Matrix,

Cryogenics, Vol. 44, pp. 439–444 (2004).

[6] The World of Industrial Wirecloth and Screens, Potter and Soar Ltd., Specialist.

[7] G.T. Lee, B.H. Kang and J.H. Lee, Effectiveness Enhancement of a Thermal Regenerator in an Oscillating Flow, Applied Thermal Engineering, Vol. 18 (8), pp. 653-660 (1998).

[8] M.K. Mittal and L. Varshney, Optimal Thermo Hydraulic Performance of a Wire Mesh Packed Solar Air Heater, Solar Energy, Vol. 80, pp. 1112–1120 (2006).

[9] Y. Timoumi, I. Tliliand and S. Nasrallah, Technical Note: Performance Optimization of Stirling Engines, Renewable Energy, Vol. 33, pp. 2134–2144 (2008).

[10] D.G. Thombare and S.K. Verma, Technological Development in the Stirling Cycle Engines, Renewable and Sustainable Energy Reviews, Vol. 12, pp. 1–38 (2008).

[11] N. Kagawa, K. Hirata, M. Takeuchi, I. Yamashita, K. Araoka, K. Hamaguchi,, Isshiki, N., Matsuo, M., Matsushita, M., Miyabe, H. and Moriya, S., Design of 100 W Stirling Engine, ICSC - 031, Tokyo, pp. 211-216 (1995).

[12] G.T. Reader and C. Hooper, Stirling Engines, University Press, Cambridge, U.K. pp. 341-359 (1983).

[13] M. Kuosa, M. Kaikko J. and L. Koskelainen, The Impact of Heat Exchanger Fouling on the Optimum Operation and Maintenance of the Stirling Engine, Applied Thermal Engineering, Vol. 27, pp. 1671–1676 (2007).

[14] G.H Martin, Kinematics and Dynamics of Machines, 2nd Edition, McGraw-Hill Book Company, Tokyo (1982).

[15] B.S. Massey, Mechanics of Fluids, Van Nostrand Reinhold (U.K.) Co. Ltd., 5th Edition (1983).

[16] W. Chung and S. Kim, Experimental Study of Heat Input System in Stirling Engine, 7th ISEC, Waseda University, Shinjuku, Tokyo, pp. 113-118 (1995).

[17] K. Tsuchiya, S. Uchida, T. Hatanaka, N. Okamura and I. Fujii, Non-Linear Pressure Drop in Heat Exchanger Element Under Periodic Flow Condition, 7th ISEC, Waseda University, Shinjuku, Tokyo, pp. 83-88 (1995).

[18] M. Tanaka, I. Yamashita and F. Chisaka, Flow and Heat Transfer Characteristics of the Stirling Engine Regenerator in an Oscillating Flow, JSME Int. Jor., Series II, Vol. 33 (2), pp. 283-289 (1990).

[19] J.P. Holman Heat Transfer, Ninth Edition, New York, McGraw-Hill Inc (2002).

[20] J.R. Senft and J.V. Senft, Dual Bell Crank Mechanisms for Stirling Engines, 7th ISEC-1995, Waseda University, Shinjuku, Tokyo, pp. 513-518.

[21] K. Hirata, Mechanical Loss Reduction of a 100 W Class Stirling Engine, 11th ISEC-2003, University of Rome, La Sapienza, Rome, pp. 338-343.

[22] K. Hirata, E. Ishimura, M. Kawada, , T. Akazawa and M. Iida, Development of a Marine Heat Recovery System with Stirling Engine Generators, 13th ISEC-2007, Waseda University, Shinjuku, Tokyo, pp. 331-336.

Received August 25, 2008
Accepted January 27, 2009